INTL JOURNAL OF ELECTRONICS AND TELECOMMUNICATIONS, 2023, VOL. 69, NO. 3, PP. 537-544
Manuscript received January 18, 2023; revised July, 2023. DOI: 10.24425/ijet.2023.146504

Performance of a Software Defined Radio based Non-Coherent OFDM Wireless Link

Nandana Narayana, and Pallaviram Sure

***Abstract*—With improved technological successions, wireless communication applications have been incessantly evolving. Owing to the challenges posed by the multipath wireless channel, radio design prototypes have become elemental in all wireless systems before deployment. Further, different signal processing requirements of the applications, demand a highly versatile and reconfigurable radio such as Software Defined Radio (SDR) as a crucial device in the design phase. In this paper, two such SDR modules are used to develop an Orthogonal Frequency Division Multiplexing (OFDM) wireless link, the technology triumphant ever since 4G. In particular, a non-coherent end-to-end OFDM wireless link is developed in the Ultra High Frequency (UHF) band at a carrier frequency of 470 MHz. The transmitter includes Barker sequences as frame headers and pilot symbols for channel estimation. At the receiver, pulse alignment using Max energy method, frame synchronization using sliding correlator approach and carrier offset correction using Moose algorithm are incorporated. In addition, wireless channel is estimated using Least Square (LS) based pilot aided channel estimation approach with denoising threshold and link performance is analyzed using average Bit Error Rate (BER), in different pilot symbol scenarios. In a typical laboratory environment, the results of BER versus receiver gain show that with 4 pilot symbols out of 128 carriers, at a gain of 20 dB, BER is 0.160922, which is reduced to 0.136884 with 16 pilot symbols. The developed link helps OFDM researchers to mitigate different challenges posed by the wireless environment and thereby strengthen OFDM technology.**

***Keywords*—Software Defined Radio (SDR); Universal Software Radio Peripheral (USRP); LabVIEW; LS channel estimation, denoising threshold**

I. INTRODUCTION

MODERN wireless services are aggressively driven towards interconnecting everyone with everything including machines, vehicles and other electronic gadgets. Underlying corroborative technological advancements have empowered today's 5G standards to support a wide variety of services including Internet of Things (IoT) [1], Vehicle to Vehicle (V2V) [2] and Machine to Machine (M2M) [3] communication systems. Whether it be a wireless application related to IoT, V2V, M2M or a wireless service such as the 5G [4], design and testing phase are very crucial before deployment.

Design phase of wireless applications mandate the availability of appropriate radio equipment, including both Radio Frequency (RF) front end as well as the baseband signal processing blocks. Inevitable design modifications to the traditional radio equipment is usually very expensive and less supportive. Hence modifying radio devices quickly and affordably has become indispensable, to cope up with the exponential growth of wireless applications. In this regard, the contemporary SDR [5] modules are very cost effective and flexible choice. The SDRs offer programmable baseband signal processing units, to support easy design modifications, while also providing a controllable RF front end that can be integrated to the baseband unit.

Cost-effectiveness, controllable RF and programmable baseband enable wireless communication technologies or applications to prosper and there by encourage the service providers, product developers as well as end users. As most of the physical layer operations are implemented using suitable software, functional enhancements are possible through software updates. Based on operating frequency and the wireless application, different SDR modules are available.

In this paper, using two such SDR modules, an end-to-end non-coherent OFDM wireless link is developed in the UHF television (TV) band at 470 MHz carrier frequency, and its performance is analyzed in terms of link BER. Starting with Fourth generation-Long Term Evolution (4G-LTE) till today's Fifth generation New Radio (5G NR) [6] and the futuristic Sixth generation (6G) [7-9], OFDM has been a very successful modulation type owing to its primary advantage of combating frequency selective fading [10] and thereby reducing Inter Symbol Interference (ISI) [11]. However, its implementation in any wireless application, needs experimental investigation prior to actual deployment, where the necessity of a suitable SDR comes into picture.

Some of the popularly available SDR modules include HackRF One, KiwiSDR, RealTek RTL-SDR, Ettus Research Universal Software Radio Peripheral (USRP) N210, USRP N200, Analog Devices Active Learning Module (ADALM)-PLUTO and National Instruments (NI) SDR modules such as USRP 2901, USRP 294x, USRP 295x. These SDRs are compatible with various programming platforms such as GNU Radio [10], Laboratory Virtual Instrument Engineering Workbench (LabVIEW), Matrix Laboratory (MATLAB).

HackRF One SDR is a half-duplex RF transceiver that supports 1 MHz to 6 GHz and is compatible with GNU Radio.

Authors are with Department of Electronics and Communication Engineering, MS Ramaiah University of Applied Sciences, Bangalore, India (e-mail: nandana.narayana@gmail.com, pallaviramsure.ec.et@msruas.ac.in).

KiwiSDR supports shortwave, longwave, and AM broadcast bands, as well as different utility stations and amateur radio transmissions from 10 kHz to 30 MHz frequency range. RTL-SDR supports frequencies between 500 kHz to 1.7 GHz, and is suitable for applications in air traffic control, general radio scanning and public safety radio. In addition to GNU Radio, RTL-SDR supports MATLAB programming. Ettus Research USRP N210 supports up to 6GHz frequency and is a high performance, fully integrated, inexpensive, single-board SDR, which is compatible with GNU Radio. ADALM PLUTO SDR is another half-duplex RF transceiver that is compatible to MATLAB and supports 325 MHz to 3.8 GHz.

The NI USRPs such as NI 294X, NI 295X and NI 2901 are another class of RF transceivers that are compatible with LabVIEW software. These USRPs support operation in wideband because of their sampling and synthesizing bandwidth, ranging from 30-120MHz, which is 1 million times greater than that of PC sound cards [5]. In this work, the NI USRP-2901 is utilized, which supports carrier frequency between 70 MHz to 6 GHz. Various experimental prototypes for different wireless applications have been built using the above said SDR modules, in the available literature. Some of these works are discussed as follows.

A common transceiver for digital modulation system at 40 MHz is demonstrated with two USRP N210 devices and GNU radio [5]. A distributed test bed for 5G scenario [12] is developed using USRP N200 programmed with GNU radio software, where Raspberry Pi3 B+ serves as a decision making engine. A video stream is transmitted to its destination using User datagram protocol (UDP) packets with multi hop transmission via 4 intermediate USRP modules. The end-to-end delay of cognitive network operating in licensed TV band frequency of 850 MHz is studied in different processing scenarios. From [5] and [12], it can be observed that SDRs support the development of a simple wireless digital link to an advanced 5G network prototype.

Some of SDR modules used in cognitive link applications are discussed as follows. In [13], using ADALM PLUTO SDR via MATLAB, a UHF TV band signal from 470-790 MHz is captured for wideband spectrum sensing in cognitive radio application. A cognitive radio link at 915 MHz, with primary and secondary user communication is developed in [14], using NI USRP 2901 and LabVIEW. A robust multiband spectrum detection method for cognitive radio is investigated [15], using four USRP modules and a mobile phone. HackRF One SDR, RTL SDR 0005 and RTL SDR 0002 are programed as receiver, whose operating frequencies are 835 MHz, 846.2 MHz, and 848.6 MHz respectively. Lime SDR mini is programed as an OFDM transmitter at 847.8MHz. OFDM based real time spectrum sensing using semi blind detectors, namely Singular Value Decomposition (SVD) based [16] and energy detector, is demonstrated using two NI USRP 2930 devices [17], at a carrier frequency of 433.92MHz, by considering both Rician and flat fading environments. A testbed for demonstrating dynamic spectrum sensing using wavelet method, is developed using USRP 2920 [18], at a carrier frequency of 2GHz.

SDRs can also be employed for IoT or WSN applications. Arduino Uno microcontroller and two USRP NI 2901 (one programmed as node and another as fusion center using LabVIEW) are used to implement a 470 MHz wireless sensor node [19], capable of acquiring and transmitting temperature and pH values of an aquaponics system to a remote fusion center.

In the available literature, some of the works that focused on OFDM wireless link development are discussed as follows. An OFDM system is demonstrated using NI USRP 2901 device and LabVIEW software [20], for Digital Audio Broadcasting (DAB), at an operating frequency of 1.5 GHz, using Four-Quadrature Amplitude Modulation (4-QAM) as the modulation scheme.

An OFDM system developed using Ettus USRP1 with MATLAB and Simulink programming [21], has incorporated an arbitrary signal generator to create two path channels and the transmitted symbols are passed through these generated channels. At the receiver the overall signal distortion has been analyzed using Modulation Error Ratio (MER). In [22], two simultaneous OFDM wireless links are established using two NI USRP 2901 devices at 910MHz, 950 MHz respectively, with 48 sub carriers and 4-QAM modulation.

An OFDM transceiver [23] is implemented using two Ettus Research USRP N210 devices, one programmed as transmitter another as receiver, and Mean Square Error (MSE) parameter is assessed. Baseband signal processing on QPSK signals is performed using MATLAB, interfaced to USRP.

Two Ettus USRP N210 modules, one personal computer (PC) and MIMO cable are used to develop an OFDM transceiver [24]. Baseband signal processing on QPSK signals and communication between two USRP N210 devices is achieved by means of LabVIEW software. A joint frame synchronization with channel estimation is investigated for multi-path frequency selective channels [24] using different sparse recovery approaches, and an equalizer is designed. The MSE between the equalized output and the transmitter symbols is used to evaluate the link performance. An OFDM system using NI USRP with LabVIEW programming [25], has studied the Peak to Average Power Ratio (PAPR) of the overall system, by using different companding techniques at a frequency of 2.5 GHz.

From the above cited works, it can be understood that in the OFDM links [23] and [24], the link BER is not investigated and different pilot symbol scenarios are not studied. Further MIMO cable has been incorporated for synchronization between the devices. A practical multipath channel is not considered in the OFDM link [21] and in addition, link BER has not been analyzed in the OFDM links [21] and [25].

In this work, we address a non-coherent OFDM wireless link and study its BER in different pilot symbol scenarios. A Barker sequence is inserted as a frame header at the transmitter that sends Quadrature Phase Shift Keying (QPSK) symbols, while frame synchronization is performed using sliding correlator method, and carrier frequency offset estimation is performed using Moose algorithm, at the receiver. In addition, unlike the above discussed works [20 - 25], this OFDM link incorporates and studies the BER performance of Least Squares (LS) channel estimation approach with denoising threshold in different pilot symbol scenarios.

The rest of the paper is organized as follows. The USRP based OFDM wireless link prototype is illustrated in section II. The details of baseband transmitter and receiver incorporated in LabVIEW is discussed in section III. Section IV discusses the experimental results of the OFDM link and section V concludes the paper.

II. OFDM Wireless Link Model using SDR

In this work, two NI USRP 2901 SDR devices, discussed in section 1 are used to develop a non-coherent end-to-end OFDM wireless link prototype, at an operating frequency of 470 MHz, as in Figure 1. The first SDR is programmed as transmitter (Tx) and the second one is programmed as receiver (Rx) using a PC with LabVIEW. The two SDRs are connected to the PC using Universal Serial Bus (USB) cables, without any external power supply. The UHF triband monopole antennas are used for communication at both Tx and Rx, which are separated by 6m distance. Gain at the transmitter is fixed at 0dB, while at receiver it is variable from (0-20)dB. Experiments were conducted in a laboratory environment, with many PCs, tables and other obstacles that constitute a typical multipath radio channel. Figure 1 also shows the PC containing LabVIEW software, where Tx and Rx baseband programming is implemented as virtual instrument (vi) files, Tx.vi and Rx.vi respectively.

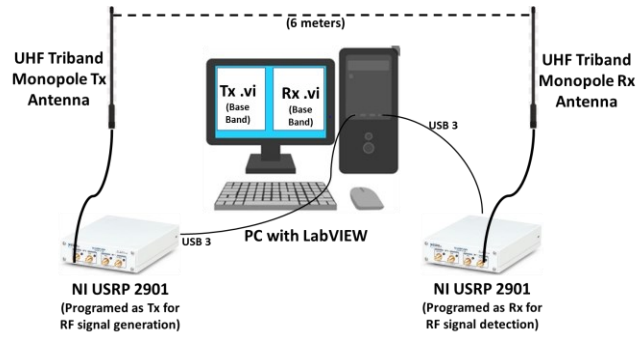

Fig. 1. OFDM Wireless link using NI USRP 2901 SDR

The RF portion provided by the SDR can be understood from the SDR block diagram shown in Figure 2, indicated as Analog RF Transceiver. Note that each SDR acts either as a Tx or an Rx, and hence the top RF chain in Figure 2 can be interpreted as analog RF Tx SDR and the bottom one as analog RF Rx SDR. As in Figure 2, the NI USRP 2901 SDR mainly comprises of two parts, analog RF transceiver and mixed function Field Programmable Gate Array (FPGA).

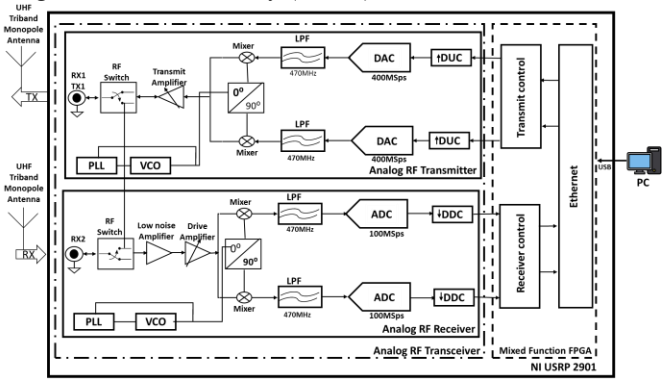

Fig. 2: RF Portion of NI-USRP 2901 [27]

Digital baseband signal generated in PC passes to the Tx path of the analog RF transceiver via the mixed function FPGA and then to UHF triband monopole antenna. The Tx path consists of Digital Up-Converter (DUC), Digital-to-Analog Converter (DAC), Low Pass Filter (LPF), mixer, transmit amplifier, Phase Locked Loop (PLL), Voltage Controlled Oscillator (VCO) and RF switch. Note that the PC synthesized baseband In-phase and Quadrature (IQ) signals are transmitted to the SDR over a USB 3.0 connection that allows a maximum data rate of 1600Mbps. The DUC block in the device up converts the signal and the DAC converts it to analog, which is fed to the LPF and then to a mixer. LPF reduces noise and high frequency components in the signal. The signals are up converted by the mixer to the chosen RF frequency of 470 MHz, where PLL locked VCO signal forms the third input. The obtained signal is amplified by transmit amplifier, before being sent to antenna via RF switch.

Received analog signals at the Rx SDR pass through the bottom RF chain in Figure 2. The received analog RF signal reaches the RF switch and is passed through the low-noise amplifier and drive amplifier, and is then down converted by the mixer to baseband IQ components, after which it passes through the LPF. The corresponding IQ signal is fed to Analog-to-Digital Converter (ADC) block, followed by decimation using Digital-Down-Converter (DDC) at desired sampling rate. The resultant samples are passed to PC over a USB 3.0 connection and are further processed in the baseband to finally obtain the transmitted baseband symbols. The details of the baseband OFDM system blocks are depicted in Figure 3.

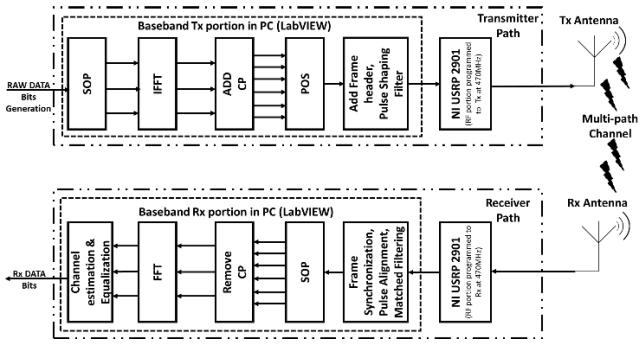

Fig. 3. Baseband OFDM Block Diagram

The baseband Tx and baseband Rx of Figure 3 are implemented in LabVIEW as Tx.vi and Rx.vi files shown in Figure 1. At the baseband Tx, raw QPSK data are generated serially and are converted to parallel using Serial to Parallel (SOP), which are then fed to Inverse Fast Fourier Transform (IFFT) block to obtain OFDM symbols, each comprising N subcarriers, out of which are P pilots (known transmissions that aid the receiver in channel estimation). Subsequently, Cyclic Prefix (CP) is added by appending the tail portion of the OFDM symbol to its beginning, in order to eliminate ISI [13]. Each resultant OFDM symbol passes through the Parallel-to-Serial (POS) block for serial transmission, followed by addition of frame header and zero padding. The resultant symbols are the pulse shaped using suitable filters and are passed to NI USRP 2901 SDR, for RF signal processing, as shown in Figure 2. Note that addition of CP reduces the receiver hardware complexity as it converts convolution between transmitted OFDM symbol and the channel impulse response (CIR) [26] to cyclic convolution.

The baseband Rx block of LabVIEW accepts the IQ symbols obtained from the RF chain of the NI USRP 2901 SDR in a serial fashion, and performs frame synchronization, pulse alignment, and matched filtering. The resultant symbols are converted to parallel using SOP block, which are FFT

processed after removing CP. Channel estimation and equalization is performed to extract the actual symbols transmitted at the baseband Tx.

III. BASEBAND IMPLEMENTATION IN LABVIEW

In this section baseband LabVIEW implementations of Tx.vi and Rx.vi shown in Figure 1, and depicted in Figure 3 are discussed. Figure 4 depicts the mixed function FPGA controls that enable interaction between Tx.vi LabVIEW file and the transmitter SDR. These are a set of four functions, *open Tx session*, *configure signal*, *write Tx data* and *close session*. The SDR device name is input to the *open Tx session* function. Using *configure signal* function, the SDR parameters are set. Here, IQ rate is set to 128k samples/second, symbol rate is set to 6400 symbols/second, carrier frequency is set to 470 MHz, transmitter gain is set to 0 dB, and further the active antenna is also set. The function accepts these values, and coerces them if they are not within the device limits, which can be displayed. The baseband data frame to be transmitted is input to *write Tx data* function. This function is kept within a while loop to enable repeated frame transmission. *Close session* function cuts-off transmission after while loop execution.

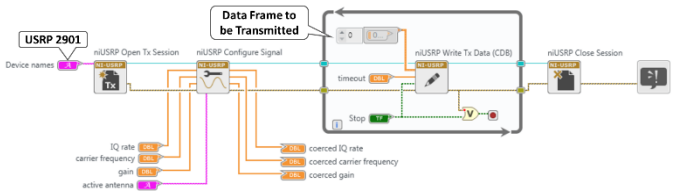

Fig. 4. Transmitter Template [27]

The data frame to be transmitted, shown in Figure 4 is generated via Tx.vi, as illustrated in Figure 5, which has different subvi blocks, each of which is discussed below.

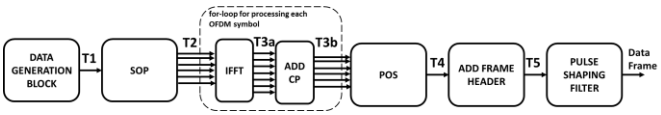

Fig. 5. Subvi Blocks of Tx.vi

The data generation block generates data frames of QPSK symbols in IQ form, $\frac{1}{\sqrt{2}}(1 \pm j)$. Each frame comprises of 640 QPSK symbols, which represent a total of 5 OFDM symbols with 128 subcarriers per symbol. *Fibonacci pseudo noise (PN) sequence generator* function generates random sequence of 1280 $(= 640 * 2)$ binary bits, with primitive polynomial order of 9. A *math script node* function accepts these binary bits, where 0 bit is converted to -1, and grouping first 640 as real and the next 640 as imaginary, a total of 640 complex QPSK symbols are obtained. The SOP block is incorporated using inbuilt *reshape* function, to convert the 640 IQ symbols to a matrix of 128×5, indicating 128 parallel transmissions per OFDM symbol. The *for* loop accepts one OFDM symbol at a time and performs IFFT using an inbuilt function. 50% CP equivalent to 64 symbols is added to the IFFT output. *Split 1D array* function is used to extract last 64 IQ symbols and these are appended to the beginning of each OFDM symbol via *insert-into-array* function. Therefore resultant time domain OFDM symbol comprises of 192 $(= 128 + 64)$ IQ symbols. Correspondingly, at T3b of figure 5, the OFDM frame size becomes 192×5, that are input to POS block after normalization. Inbuilt *reshape* function is used in POS block to obtain 960 $(= 192 \times 5)$ serial transmissions. In the Add frame header subvi block, a 26 length QPSK Barker sequence is generated as a frame header via *math script node* function. Further using, *insert into array* function, the frame header is appended to the 960 length CP added data frame. Thus the frame length at T5 is $986 (= 960 + 26)$.

Pulsed shaping filter block comprises of 3 functions. The input 986 complex binary bits are sent to *upsample* function, whose sampling factor is set to 20 samples/symbol. Note that this factor is the ratio of IQ rate and symbol rate. The resultant data frame has now a length of 19720 $(= 986 * 20)$ samples. The frame now gets convolved with the output from *generate filter coefficient* function using *convolution function*. The *generate filter coefficient* function is chosen as root raised cosine with filter length of 8 and 20 pulse shaping samples/symbol. Hence the convolved normalized output is a frame of length 19880$\big(= 19720 + (8 * 20)\big)$ samples, which is equivalent to a frame duration of 0.155 seconds. This data frame is fed to *write Tx data* function of Figure 4. Note that due to normalization the signal values in the data frame range from -1 to +1 only. Increasing the set transmitter gain, the strength of the signal increases.

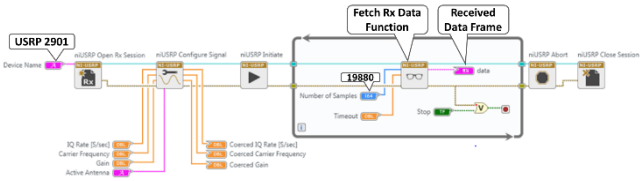

Fig. 6. Receiver Template [27]

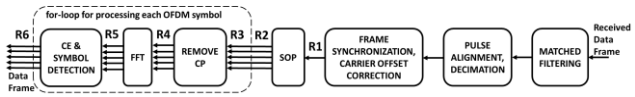

Fig. 7. Subvi Blocks of Rx.vi

The Rx.vi shown in Figure 1, depicted in Figure 3 is discussed next. Figure 6 depicts the mixed function FPGA controls that enable interaction between Rx.vi LabVIEW file and the receiver SDR. These are a set of 6 functions, *open Rx session, configure signal, initiate, fetch Rx data, abort* and *close session*. The *open Rx session* function seeks device (SDR) name. The *configure signal* function has the same functionality as that of the transmitter's function. The receiver gets initiated via the *initiate* function. The *fetch Rx data* function, acquires the received data frame with specified number of samples. This function is shown inside the while loop to indicate repeated frame reception. Finally, after the while loop execution, the *abort* function halts the data frame collecting process, and the receiver operation halts via *close session* function. The received data frame shown in Figure 6, is passed to Rx.vi file for baseband signal processing and subsequent symbol detection, as illustrated in Figure 7 in the form of 5 subvi blocks.

In order to facilitate proper frame retrieval, the number of samples input to *fetch Rx data* function is set as length of 3 data frames ($= 3 * 19880$).

The received data frame in Figure 6, is input to matched filtering subvi, to maximize the Signal to Noise Ratio (SNR). Corresponding output is obtained by convolution of root raised cosine impulse response $h(n)$ of length 161 (=(20 samples/symbol * raised cosine filter length of 8)+1) and received data frame. Owing to the non-coherent nature of the wireless link, pulse alignment and frame synchronization are imperative. The pulse alignment block incorporates max energy method [19]. Accordingly, its input is decimated by a factor D =20 samples/symbol, and the resultant decimated signal $m(n)$ is used to calculate signal energy as

$$P(d) = \mathbf{E}\{|m(n+d)|^2\} \quad (1)$$

where d is the delay ranging from 0 to $(D-1)$, and the expectation operator in (1) can be replaced by a summation as in

$$P(d) = \frac{1}{N}\sum_{n=0}^{N-1}|m(n+d)|^2 \quad (2)$$

The delay at which $P(d)$ becomes maximum, is the actual pulse position. The pulse aligned signal is then decimated to obtain the received data frame, which is passed to frame synchronization and carrier offset correction subvi. Sliding correlator approach [19, 28] is used for frame synchronization. This approach utilizes training sequences such as Ergo sequences by Gold, Zadoff-Chu, Frank, or Barker [19, 28] as headers. Note that 2 Barker sequences of length B_h=13, namely {0,0,0,0,0,1,1,0,0,1,0,1,0} are concatenated to obtain the $B = 26$ length frame header which is inserted at the transmitter, referred as $b(n)$. Let the received 26 length frame header be $d(n)$. Cross correlation is computed as

$$J(k) = |\sum_{n=0}^{B-1} b^*(n)d(n+k)|^2 \quad (3)$$

The value of k corresponding to the first maximum of $J(k)$ represents the frame offset. The frame synchronized data is then corrected for carrier offset, using Moose algorithm, where the periodicity B_h of the header sequence is utilized. Received data frame $r(n)$ comprising an offset can be expressed [19] as

$$r(n) = e^{j2\pi f_{OFF}(nT_S)}\sum_{i=0}^{L_t-1} h(i)\, s(n-i) + w(n) \quad (4)$$

where, $w(n)$ is the Additive white Gaussian noise (AWGN), frequency offset is f_{OFF} and the sampling time is T_s, channel length is L_t and $s(n)$ is the actual transmitted data frame and $h(n)$ is the channel impulse response of the multipath wireless channel. Limiting $r(n)$ in (4) to the received header portions, and there by replacing $s(n)$ with $d(n)$, where $d(n) = d(n + B_h)$, the received header $r_h(n)$ can be expressed as

$$\begin{aligned} r_h(n+B_h) &= e^{j2\pi\epsilon(n+B_h)}\sum_{i=0}^{L_t-1} h(i)\, d(n+B_h-i) + w(n+B_h) \\ &\approx e^{j2\pi\epsilon B_h} r_h(n) \end{aligned} \quad (5)$$

where $= f_{OFF}T_s$. Formulating (5) as a minimization problem

$$\min_a \sum_{i=L_t}^{B_h-1}|r_h(i+B_h) - a r_h(i)|^2 \quad (6)$$

where $a = e^{j2\pi\epsilon B_h}$ can be estimated [19] as

$$\hat{a} = \frac{\sum_{i=L_t}^{B_h-1} r_h(i+B_h) r_h{}^*(i)}{\sum_{i=L_t}^{B_h-1}|r_h(i)|^2} \quad (7)$$

As only phase of $\hat{a}$ is required for offset correction, we obtain

$$2\pi\hat{\epsilon}B_h = Phase\left(\sum_{i=L_t}^{B_h-1} r_h(i+B_h) r_h{}^*(i)\right) \quad (8)$$

and subsequently $\hat{f}_{OFF} = \frac{\hat{\epsilon}}{T_s}$ can be substituted in (4), to obtain the offset corrected received data frame as

$$r_{OFF}(n) = e^{-j2\pi\hat{f}_{OFF}(nT_S)} r(n) \quad (9)$$

The 26 length header is discarded from $r_{OFF}(n)$ in (9), to obtain desired $L_t = 960$ length data frame. This frame is passed to SOP subvi block, where inbuilt *reshape array* function is used to obtain 192×5 data frame. The output of SOP block at R2 is input to the *for* loop. One OFDM symbol of 192 length, passes to the loop at a time. Using *split 1D array* function, the first 64 length of 192 length OFDM symbol is discarded in the remove CP block, and 128 length OFDM symbol is passed to FFT block to obtain the transmitted data symbols. Owing to the multipath fading environment, the channel estimation and symbol detection block is incorporated to nullify the channel's effect. LS channel estimation with a denoising threshold [10] is incorporated using *math script node* function. Consider one OFDM symbol after the FFT block, which can be expressed as

$$r_{OFF}(k) = s(k)h_f(k) + w(k) \quad (10)$$

where k is the subcarrier index ranging from 0 to 127, $h_f(k)$ is the Fourier transformed channel frequency response of $h(n)$, and $s(k)$ represents transmitted QPSK symbols of the considered OFDM symbol. Retaining only the pilot positions, (10) is rewritten as

$$r_{OFF,p}(k) = s_p(k)h_{f,p}(k) + w_p(k) \quad (11)$$

where p indicates the subcarrier position, If total number of pilot symbols is P_s, using channel length L_t and the Fourier relation of $h_{f,p}(k)$, (11) can be expressed in matrix form as

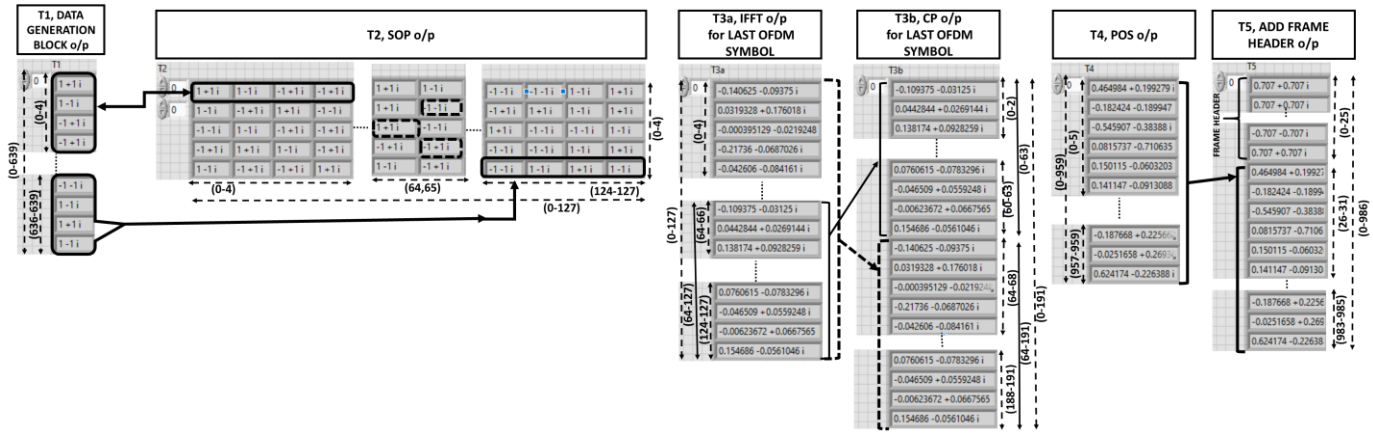

Fig. 9. Results of Transmitter in Figure 5

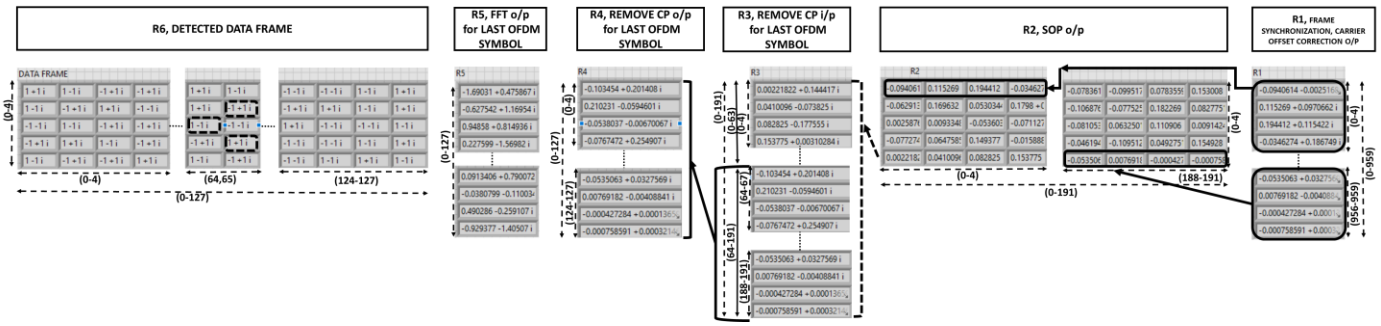

Fig. 11. Results of Receiver in Figure 7

$$\boldsymbol{r}_p = \mathbf{S}_p\mathbf{F}_p\boldsymbol{h} + \boldsymbol{w}_p \tag{12}$$

where, $\boldsymbol{r}_p \in \mathbb{R}^{P_s\times 1}$, $\mathbf{S}_p$ is a diagonal matrix, with diagonal positions occupied by transmitted pilot symbols, $\mathbf{F}_p \in \mathbb{R}^{P_s\times L_t}$ is the Fourier matrix formed by retaining only the first L_t columns, $\boldsymbol{h} \in \mathbb{R}^{L_t\times 1}$ is the channel impulse response that needs to be estimated. LS approach estimates $\boldsymbol{h}_p$ [29] as

$$\widehat{\boldsymbol{h}} = \left(\mathbf{S}_p\mathbf{F}_p\right)^{\dagger}\boldsymbol{r}_p \tag{13}$$

where $(.)^{\dagger}$ indicates the Moore Penrose pseudo inverse matrix. On $\widehat{\boldsymbol{h}}$, a denoising threshold is applied to obtain better channel estimate, which is $2\sigma_v^2$, where σ_v^2 is the noise variance estimate as in [10]. The channel estimate after thresholding say $\widehat{\boldsymbol{h}}_{th}$ is used to estimate the channel frequency response as $\boldsymbol{h}_f = \mathbf{F}\widehat{\boldsymbol{h}}_{th}$, where $\mathbf{F} \in \mathbb{R}^{N\times L_t}$ is the Fourier matrix retaining only the first L_t columns. The symbol detection is there by performed as follows. Using (10), at the non-pilot subcarrier positions, the detected symbols can be obtained via zero forcing [10] as

$$\hat{s}(k) = sign(r_{OFF}(k)/h_f(k)) \tag{14}$$

where k indicates the data positions, and $sign(.)$ indicates signum function applied on both real part and imaginary part separately. The thus obtained QPSK symbols $\hat{s}(k)$ form the received OFDM data symbols at R6 in Figure 7.

IV. Results and Discussion

The OFDM wireless link shown in Figure 1 is established in a laboratory, a snap of which is shown in Figure 8. The stage wise results of Tx.vi, given in Figure 5 are shown in Figure 9. Output at T1 is complex QPSK data of size 640×1, which is converted into parallel at T2, having a size 128×5, indicating 5 OFDM symbols with 128 subcarriers each. For better observation factor of $\left(\frac{1}{\sqrt{2}}\right)$ is removed from the display of QPSK symbols. Observe that serial symbols from row (0-4) of T1 came out as first row, (0-4) columns in T2, and similarly row symbols from (636-639) of T1 are transferred to last row as (124-127) columns in T2. After T2 is fed as one OFDM symbol per iteration into *for* loop in Figure 5, the output at T3a of size is 128×1 and at T3b of size 192×1 after addition of CP are also depicted. Note that T3b is attained by affixing row (64-127) from T3b to its beginning (0-63). The rest of the OFDM symbol row (64-191) is same as row (0-127) of T3a. Observe that symbols in row (0-4) of T3a are same as (64-68) of T3b, row (64-66) of T3a is same as (0-2) of T3b, row (124-127) of T3a is same as (188-191) and (60-63) of T3b. Next, the 128×5 output is transformed to frame of 960 serial symbols at T4.

Then QPSK frame header of size 26×1 is added to start of the frame to obtain T5 of size 986×1. It can be observed that row (0-5) of T4 is same as (26-31) of T5, row (957-959) of T4 is same as (983-985) of T5. The result of pulse shaping on T5 is shown in Figure 10, which is the data frame to be transmitted and fed to write Tx data function discussed in section 3. Note that due to normalization, signal strength ranges between +1 and -1 and start of the transmitted IQ signal is a QPSK Barker sequence.

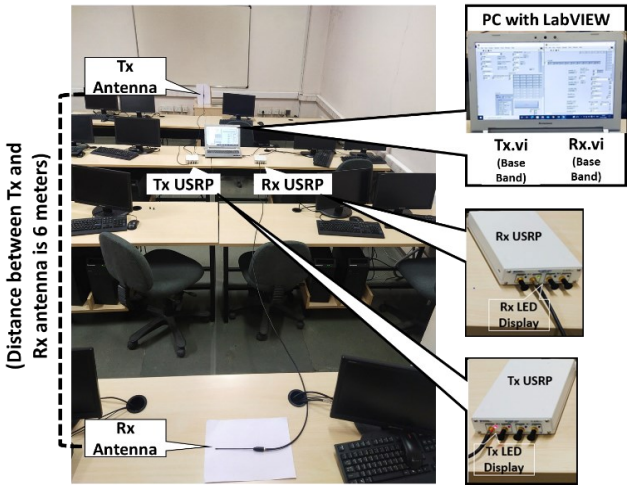

Fig..8. The non-coherent OFDM wireless link

The stage wise results of Rx.vi in Figure 7 are shown in Figure 11. Output at R1 consists of 960×1 complex QPSK symbols, converted to parallel 5×128 sized matrix at R2. Rows (0-4) of R1 are same as first row (0-4) columns in R2, and rows (956-959) of R1 are same as last row (188-191) columns in R2. The results of the last OFDM symbol is considered, to depict results inside the *for* loop. Last row of R2 is input to Remove CP block. Note that last row (0-4) columns of R2 are same as (0-4) rows in R3 and last row (188-191) columns of R2 are same as (188-191) in R3. After CP removal, R4 has 128 length which is extracted from rows (64-191) of R3. FFT on R4 leads to R5 of 128 length, which is input to channel estimation and symbol detection block. This block output at R6 is compared with transmitted data frame, T2 of Figure 9 to check for errors, and these frames are later used for BER calculation. Few errors are highlighted using dashed-squares in columns 64 and 65 of T2 and R6, in Figure 9 and Figure 11 respectively.

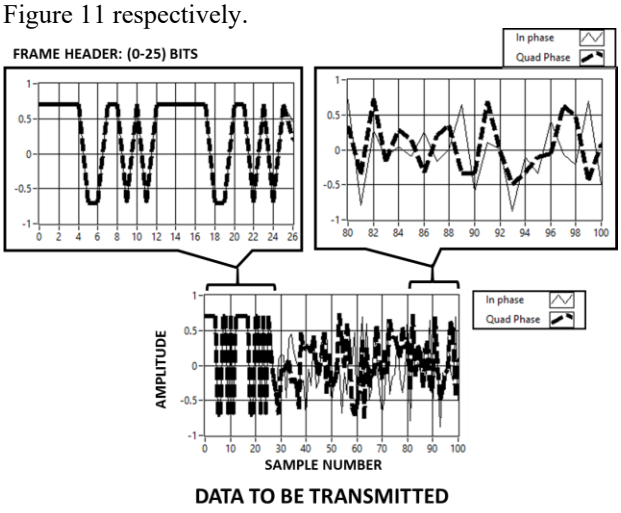

Figure 10: Transmitted IQ signal

By varying receiver gain from 0 dB to 20 dB, 250 OFDM frames are received for each gain setting, which are used for average BER computation. For 128 subcarrier OFDM symbol, Figure 12 shows average BER versus receiver gain for different pilot symbol scenarios namely, $P = 4$ and $P = 16$. Note that length of the channel $L_t = 20$, and the maximum number of non-zero channel taps are observed as close to 6 for the laboratory environment considered. The BER results show that more the number of pilots, better is the BER. Thus for $P = 16$ scenario, BER is better.

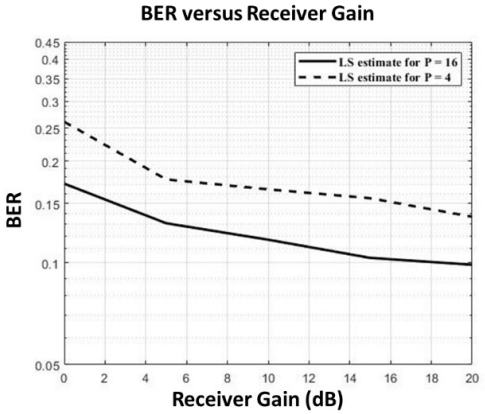

Figure 12: BER versus SNR

Figure 13 displays channel impulse responses at 20dB receiver gain for both $P = 16$ and $P = 4$ obtained using LS estimate. Note that $P = 4$ case represents a severe pilot reduction scenario with pilot spacing of 32 and also overhead is less but BER suffers. Further, $P = 16$ case indicates a pilot spacing of 8 with more overhead but better BER. Thus a trade-off is always necessary between BER and overhead in practice.

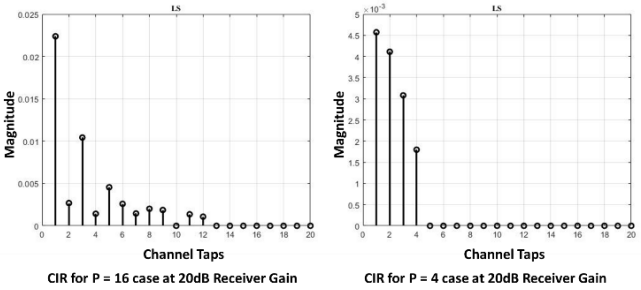

Figure 13: Channel Impulse Response

V. CONCLUSIONS

In this work, a non-coherent OFDM wireless link has been developed in the UHF band, utilizing two SDR modules, NI USRP 2901 with LabVIEW software. The overall link is tested at 470 MHz in a typical laboratory environment and is analyzed for its BER performance in different pilot symbol scenarios, employing LS with denoising threshold based channel estimation and a zero forcing approach for symbol detection. The obtained average BER versus receiver gain experimental plots suggest that as number of pilot symbols increase, BER reduces at the cost of overhead. Investigation on channel estimation approaches incorporating compressive sensing and sparse recovery, to obtain an improved BER performance even in severely pilot reduced scenario and thus becomes more attractive for 5G scenarios, forms the future scope of this work.

ACKNOWLEDGEMENT

We would like to express our gratitude to MS Ramaiah University of Applied Sciences, ECE department for allowing us to use the USRP NI 2901 devices, LabVIEW software and the laboratory facilities to carry out this research work. Through

a funded project, GRD-732 which is approved by VGST Karnataka under the RGS-F 2017 scheme, these devices where procured in 2019. In light of this, we also wish to thank the funding source, VGST Karnataka.

REFERENCES

[1] Khanh, Q. V., Hoai, N. V., Manh, L. D., Le, A. N., Jeon, G.: Wireless communication technologies for IoT in 5G: vision, applications, and challenges. Wireless Communications and Mobile Computing (2022).

[2] Daddanala, R., Mannava, V., Tawlbeh, L. A., Al-Ramahi, M.: Vehicle to Vehicle (V2V) Communication Protocol: Components, Benefits, Challenges, Safety and Machine Learning Applications. arXiv preprint arXiv:2102.07306 (2021).

[3] Lokhande, Meghana P., Dipti Durgesh Patil.: Secured energy efficient machine-to-machine communication for telerobotic system. Informatics in Medicine Unlocked 26. 100731 (2021).

[4] Conceição, F., Gomes, M., Silva, V., Dinis, R., Silva, A., Castanheira, D.: A survey of candidate waveforms for beyond 5G systems. Electronics. 10(1), 21 (2020).

[5] Muslimin J, Asnawi AL, Ismail AF, Jusoh AZ. SDR-based transceiver of digital communication system using USRP and GNU radio. In2016 International Conference on Computer and Communication Engineering (ICCCE) 2016 Jul 26 (pp. 449-453). IEEE. https://doi.org/10.1109/ICCCE.2016.100

[6] Levanen T, Li Z, Talvitie J, Renfors M, Valkama M. Filtered OFDM based URLLC in 5G new radio: Principles and performance. In2019 IEEE Wireless Communications and Networking Conference Workshop (WCNCW) 2019 Apr 15 (pp. 1-7). IEEE. https://doi.org/10.1109/WCNCW.2019.8902844

[7] Damjancevic, S.A., Matus, E., Utyansky, D., van der Wolf, P. and Fettweis, G.P., 2021. Channel estimation for advanced 5G/6G use cases on a vector digital signal processor. *IEEE Open Journal of Circuits and Systems*, *2*, pp.265-277, 2021.

https://doi.org/10.1109/OJCAS.2020.3047007

[8] Jiang, W., Han, B., Habibi, M.A. and Schotten, H.D., 2021. The road towards 6G: A comprehensive survey. *IEEE Open Journal of the . Communications Society*, *2*, pp.334-366.

https://doi.org/10.36227/techrxiv.13382765.v2

[9] Hong, E.K., Lee, I., Shim, B., Ko, Y.C., Kim, S.H., Pack, S., Lee, K., Kim, S., Kim, J.H., Shin, Y. and Kim, Y., 2022. 6G R&D vision: Requirements and candidate technologies. *Journal of Communications and Networks*, *24*(2), pp.232-245.

[10] Sure, P., Bhuma, C. M.: A survey on OFDM channel estimation techniques based on denoising strategies. Engineering Science and Technology, an International Journal. 20(2), 629-636 (2017).

[11] Sure, P., Bhuma, C. M.: Weighted-noise threshold based channel estimation for OFDM systems. Sadhana. 40(7), 2111-2128 (2015).

[12] Chamran MK, Yau KL, Noor RM, Wong R. A Distributed Testbed for 5G Scenarios: An Experimental Study. Sensors. 2019 Dec 19;20(1):18.

[13] P. H. Raghavendra, R. S. S. Thejaswini, K. Venugopal, M. Preethish Kumar, J. Niveditha and P. Sure, "Wideband Spectrum Sensing using Sub-Nyquist Sampling Approaches," 2020 IEEE 3rd 5G World Forum (5GWF), 2020, pp. 69-74,

https://doi.org/10.1109/5GWF49715.2020.9221076

[14] "A testbed design of Spectrum Management in cognitive radio network using NI USRP and LabVIEW" (2019) *International Journal of Recent Technology and Engineering*, 8(2S8), pp. 1828–1834. Available at: https://doi.org/10.35940/ijrte.b1164.0882s819

[15] Molina-Tenorio Y, Prieto-Guerrero A, Aguilar-Gonzalez R. Real-time implementation of multiband spectrum sensing using SDR technology. Sensors. 2021 May 18;21(10):3506.

[16] F. Z. El Bahi, H. Ghennioui, and M. Zouak, "Spectrum Sensing Technique for Cognitive Radio of Multiple OFDM Signals based on Singular Value Decomposition," in International Conference on Wireless Networks and Mobile Communications (WINCOM16). IEEE, 2016, pp.1–5

[17] El Bahi FZ, Ghennioui H, Zouak M. Real-time spectrum sensing of multiple OFDM signals using low cost sdr based prototype for cognitive radio. In2019 15th International Wireless Communications & Mobile Computing Conference (IWCMC) 2019 Jun 24 (pp. 2074-2079). IEEE. https://doi.org/10.1109/IWCMC.2019.8766788

[18] Perumal KD, Kanmani Ruby ED, Dhivya M, Aloy Anuja Mary G, Kavitha V, Kandasamy U. Experimental Analysis Using USRP for Novel Wavelet-Based Spectrum Sensing for 2.2 GHZ Band Communication Using LabVIEW. Journal of Nanomaterials. 2022 Jun 6;2022. https://doi.org/10.1155/2022/4947224

[19] Nandesh, O.N., Shetty, R., Alva, S., Paul, A., Sure, P.: A USRP based UHF Wireless Sen-sor Node and Fusion Centre for Aquaponics System Monitoring. In 2022 3rd International Conference for Emerging Technology (INCET). (1-7). IEEE (2022). https://doi.org/10.1109/INCET54531.2022.9824436

[20] Telagam N, Sahu PC, Panda S, Kandasamy N. USRP Based Digital Audio Broadcasting Using OFDM in Virtual and Remote Laboratory. Int. J. Online Biomed. Eng.. 2019 Sep 30;15(13):77-85.

[21] Tichy M, Ulovec K. OFDM system implementation using a USRP unit for testing purposes. InProceedings of 22nd International Conference Radioelektronika 2012 2012 Apr 17 (pp. 1-4). IEEE.

[22] Telagam N, Reddy S, Nanjundan M, Nehru K. USRP 2901 Based MIMO-OFDM Transciever in Virtual and Remote Laboratory. International Journal of Computer Sciences and Engineering. 2018 Jul. https://doi.org/10.26438/ijcse/v6i7.10661073

[23] Özdemir Ö, Hamila R, Al-Dhahir N, Güvenç I. Sparsity-aware joint frame synchronization and channel estimation: Algorithm and USRP implementation. InMILCOM 2017-2017 IEEE Military Communications Conference (MILCOM) 2017 Oct 23 (pp. 647-652). IEEE.

[24] Ozdemir, Ö, Anjinappa, C. K., Hamila, R., Al-Dhahir, N., Güvenç, I.: Joint frame synchronization and channel estimation: Sparse recovery approach and USRP implementation. IEEE Access. 7, 39041-39053 (2019).

[25] Kamatham, Y., Pollamoni, S.: Implementation of OFDM system with companding for PAPR reduction using NI-USRP and LabVIEW. In 2019 IEEE international WIE conference on electrical and computer engineering (WIECON-ECE). (1-4). IEEE (2019). https://doi.org/10.1109/WIECON-ECE48653.2019.9019946

[26] Coleri, S., Ergen, M., Puri, A., Bahai, A.: Channel estimation techniques based on pilot arrangement in OFDM systems. IEEE Transactions on broadcasting. 48(3), 223-229 (2002).

[27] Dr. Bruce Black (no date) *INTRODUCTORY COMMUNICATIONS SYSTEMS*, *Lab 1: Introduction to the USRP - National Instruments*. Available at: https://education.ni.com/teach/resources/5/lab-1-introduction-to-the-usrp (Accessed: November 1, 2022).

[28] Heath, R.W., 2012. Digital Wireless Communication: Physical Layer Exploration Lab Using the NI USRP: Student Lab Manual. National Technology & Science.

[29] Sure P, Bhuma CM. Large random matrix-based channel estimation for massive MIMO-OFDM uplink. IET Communications. 2018 Jun;12(9):1035-41.